

# Quantifying Effects of Earth Orbital Parameters and Greenhouse Gases on Mid-Holocene Climate

Yibo Kang and Haijun Yang\*

Department of Atmospheric and Oceanic Sciences and Institute of Atmospheric Science and CMA-FDU Joint

Laboratory of Marine Meteorology, Fudan University, Shanghai, 200438, China.

Shanghai Scientific Frontier Base for Ocean-Atmosphere Interaction Studies, Fudan University, Shanghai 200438, China.

Correspondence to: Haijun Yang ([yanghj@fudan.edu.cn](mailto:yanghj@fudan.edu.cn))

**Abstract.** The mid-Holocene (MH) is the most recent typical climate period, and a ~~hot topics~~ subject of great interest for ~~in~~ global paleocultural research. Following the latest Paleoclimate Modelling Intercomparison Project ~~phase 4~~ (PMIP4) protocol and using a fully coupled climate model, we simulated the climate ~~difference~~ ~~during~~ ~~between~~ both the MH and the pre-industrial (PI) periods, and quantified the effects of Earth orbital parameters (ORB) and greenhouse gases (GHG) on climate ~~difference~~. ~~More attention was paid to~~ ~~focusing on~~ the simulated differences in the Atlantic meridional overturning circulation (AMOC) between these two periods. Compared to the PI ~~condition~~ ~~simulation~~, the ORB effect in the MH simulation led to ~~the~~ seasonal enhancement of temperature, consistent with previous findings. ~~For~~ ~~In~~ the MH simulation, the ORB effect led to a remarkably warmer climate in the ~~mid~~ ~~high~~ ~~mid-to-high~~ <sup>21</sup> latitudes and increased precipitation in the Northern Hemisphere, which were partially offset by the cooling effect of the lower GHG. The AMOC in the MH simulation was about 4% stronger than that in the PI ~~condition~~ ~~simulation~~. The ORB effect led to 6% enhancement of the AMOC in the MH simulation, which was, however, partly neutralized by the GHG effect. ~~Transient simulation from the MH to the PI experiments further demonstrated~~ ~~the~~ opposite effects of ORB and GHG, which played opposite roles on the evolution of the AMOC ~~during the past 6000 years~~ ~~from the MH to PI~~. The simulated stronger AMOC in the MH was mainly due to the thinner sea ice in the polar oceans caused by the ORB effect, which reduced the freshwater flux export to the subpolar Atlantic and resulted in a more saline North Atlantic. This study may help us quantitatively understand the roles of different external forcing factors in ~~the~~ Earth's climate evolution since the MH.

**Keywords:** ~~M~~id-Holocene, Earth orbital parameters, Greenhouse gases, ~~A~~tlantic ~~M~~eridional ~~O~~verturning ~~C~~irculation

28 **1. Introduction**

29 The mid-Holocene (MH<sub>25</sub> 6000 years before the present) is a period of profound cultural transition worldwide,  
30 particularly in the arid-semi-arid belt of ( $\sim 30^{\circ}\text{N}$ ) (Sandweiss et al., 1999; Moss et al., 2007; Roberts et al., 2011;  
31 Warden et al., 2017). The MH climate, which belongs to the Holocene climatic optimum (Rossignol-Strick, 1999;  
32 Chen et al., 2003; Zhang et al., 2020), is significant different differs notably -from that of the subsequent period. Many  
33 studies have shown that the development of human civilization during this period was influenced by the climate,  
34 which was closely related to external factors such as the Earth's orbital parameters (ORB), greenhouse gases (GHG)<sub>2</sub>,  
35 and solar constants (Jin, 2002; Wanner et al., 2008; Warden et al., 2017). Therefore, it is of great interest to study the  
36 MH climate, for a better understanding of the influence of external forcing factors on human civilization.

37 As the key benchmark period of the Paleoclimate Modelling Intercomparison Project (PMIP) program, starting  
38 with the earliest PMIP program (Joussaume and Taylor, 1995; Kageyama et al., 2018), the MH experiment was  
39 designed to examine the climate response to a change in the seasonal and latitudinal distribution of incoming solar  
40 radiation caused by known changes in Earth orbital forcing. As the program evolved, the GHG concentrations used in  
41 the MH experiments are closer to the true values (Monnin et al., 2001, 2004). However, most studies focused on the  
42 general climate differences between the MH and pre-industrial (PI) periods; the individual effects of the ORB and  
43 GHG on the climate itself are not isolated. Some studies examined the role of GHG by comparing the different PMIP  
44 programs. Otto-Bliesner et al. (2017) found that the change in the experimental protocol between PMIP phase 4 and  
45 PMIP phase 3 (PMIP4 and PMIP3 hereafter, respectively), with a reduction in CO<sub>2</sub> concentration from 280 to 264.4  
46 ppm, would reduce GHG forcing by about 0.3 W/m<sup>2</sup>. This change can produce an estimated global mean cooling in  
47 surface air temperature (SAT) of about  $-0.28^{\circ}\text{C}$  based on the climate sensitivity of each difference models in PMIP4  
48 (Brierley et al., 2020). Note that the differences in the MH experiments between PMIP4 and PMIP3 include only the  
49 GHG effect: the The GHG contribution to temperature change is small, but not negligible although it is small.  
50 Quantifying the effects of ORB and GHG on the difference between the MH and PI is much needed. Explaining this  
51 issue clearly has important implications for a deeper understanding of the roles played by external forcing factors in  
52 the past climate.

53 The Atlantic meridional overturning circulation (AMOC) is considered an important heat transmitter of the  
54 Earth's climate system, which affects global climate on multiple various timescales (Rahmstorf, 2006). Paleoclimate  
55 studies showed that the weakening or stopping of the AMOC will lead to a large scale drastic cooling in the Northern  
56 Hemisphere (NH) can result in substantial cooling across the Northern Hemisphere (NH) –(Brown and Galbraith,  
57 2016; Yan and Liu, 2019). In recent years, predictions concerning the future behavior of the AMOC by the

58 Intergovernmental Panel on Climate Change (IPCC) are accompanied by notable uncertainties, particularly due to the  
59 substantial variability in anticipated AMOC changes under different emission scenarios (Fox-Kemper et al., 2021).  
60 Therefore, simulating past AMOC changes and exploring the effects of different forcing factors on its  
61 behavior~~studying past AMOC changes~~ will help us understand the nature of abrupt climate change in the past and  
62 better predict future climate mitigate uncertainties in future climate projections. In the previous MH simulations of the  
63 PMIP, the AMOC ~~is~~was generally stronger than that of the PI (Găinușă-Bogdan et al., 2020).~~is~~ this change in the  
64 AMOC is related to sea ice feedback, and~~but~~ these simulation results may be slightly different due to model or  
65 resolution differences (Shi and Lohmann, 2016; Shi et al., 2022). Recent studied suggested that the difference of the  
66 AMOC between the MH and PI periods in PMIP4 ensemble simulation is not significant (Brierley et al., 2020). By  
67 comparing the strength of the AMOC during the interglacial period, it was found that the variation range of the  
68 AMOC in the MH is within the internal variability range of all models; and the ORB does not seem to have played a  
69 role (Jiang et al., 2023a). Jiang et al. (2023b) also By examining used multi-model transient simulations that; all  
70 including two or more external forcing factors, and~~Jiang et al. (2023b) further found reported that the AMOC did not~~  
71 change much from the MH to the PI, which~~is~~was consistent with some proxy reconstructions.

72 In this paper, we further study the mechanism of weak difference of the AMOC between the MH and PI periods.  
73 The effects of different external forcings ~~factors~~ on the AMOC ~~will~~are ~~be~~ quantified through several sensitivity ~~In~~  
74 addition to the equilibrium experiments. Besides, M~~multiple~~ transient experiments will~~are~~ also be performed  
75 simultaneously to verify the roles of different forcing factors in long-term climate evolution. This paper is  
76 organized~~structured~~- as follows. An introduction to the fully coupled climate model is given in section 2, along with  
77 ~~the experimental~~s design. ~~The effects of ORB and GHG on the MH climate, the AMOC, and Hadley cell are shown in~~  
78 ~~section 3. In~~ s~~Section~~ 3, we presents the effects of ORB and GHG on the MH climate, ~~as well as~~and their effects on  
79 ~~the Hadley cell and the~~ AMOC, and also includes the results of transient experiments on AMOC simulations. The  
80 changes of North Atlantic Ocean buoyancy between the MH and PI periods in both equilibrium and transient  
81 experiments are described in section 4. Summary and discussion are given in section 5.

82

## 83 2. Model and experiments

84 The coupled model used in this study is the National Centre for Atmospheric Research's Community Earth  
85 System Model version 1.0 (CESM1.0) ~~is used in this study. The coupled model~~It includes atmospheric, oceanic, sea-  
86 ice, and land model components. The atmospheric model ~~has~~consists of 26 vertical levels and ~~has a~~ T31 horizontal

87 resolution (roughly  $3.75^\circ \times 3.75^\circ$ ). The land model ~~has shares~~ the same horizontal resolution as the atmospheric  
88 model. The ocean model has 60 vertical levels, and ~~employs~~ gx3v7 horizontal resolution. ~~In the zonal direction, the~~  
89 ~~grid has a uniform  $3.6^\circ$  spacing. In the meridional direction, the grid is nonuniformly spaced: it is  $0.6^\circ$  near the~~  
90 ~~equator, and gradually increases to the maximum  $3.4^\circ$  at  $35^\circ\text{N/S}$ , and then decreases poleward.~~ The sea-ice model has  
91 the same horizontal resolution as the ocean model. More details on these model components can be found in a number  
92 of studies (Smith and ~~Entregory~~, 2010; Hunke and Lipscomb, 2010; Lawrence et al., 2012; Park et al., 2014).

93 To quantify the effects of ORB and GHG on climate differences between the MH and PI periods, we designed  
94 three ~~sensitivity~~ experiments following the PMIP4 protocol (Table 1). ~~Experiment~~ MH uses the ORB and GHG in the  
95 MH period. ~~Experiment~~ MH\_ORB uses the ORB in the MH period and the GHG in the PI period. ~~Experiment~~ PI uses  
96 the ORB and GHG in the PI period. ~~Note that our simulations do not intend to reproduce the comparison climate~~  
97 ~~states between PMIP3 and PMIP4, but; we want to isolate the individual effects of ORB and GHG within the~~  
98 ~~framework of the PMIP4. There are differences between PMIP3 and PMIP4 in solar constant and GHG~~  
99 ~~concentration. The solar constant in the three equilibrium experiments simulations is set to  $1360.75\text{ W/m}^2$ . The~~  
100 ~~specific values of the Earth orbital parameters ORB- are listed in Table 1 (Berger and Loutre, 1991)-, and the GHG~~  
101 ~~data comes from the ice-core records of the Antarctica and Greenland (Otto-Bliesner et al., 2017).- The vernal equinox~~  
102 ~~is set to noon on 21 March, and the solar constant is set to  $1360.75\text{ W/m}^2$  in all three simulations. The GHG data~~  
103 ~~comes from the ice-core records of the Antarctica and Greenland (Otto-Bliesner et al., 2017). Experiments~~ MH and  
104 ~~MH\_ORB start from the PI condition, and each of the all~~ The three experiments ~~is~~ are all integrated for 2000 years ~~and~~  
105 ~~reaches the equilibrium by then (Fig. 5a).- with MH and MH\_ORB starting from the PI condition. In this paper, we~~  
106 ~~use the monthly mean data of the last 500 years of each model simulation.~~ The effect of ORB is obtained by  
107 subtracting ~~the~~ Exp PI from ~~the~~ Exp MH\_ORB, and the effect of GHG is obtained by subtracting ~~the~~ Exp MH\_ORB  
108 from ~~the~~ Exp MH. The combined effect of ORB and GHG is obtained by subtracting ~~the~~ Exp PI from ~~the~~ Exp MH. ~~In~~  
109 ~~this paper, we use the monthly mean data of the last 500 years of each model simulation for analysis after all runs have~~  
110 ~~reached equilibrium (Fig. 5a).~~

111 ~~In order to~~ To enhance the rigor of our study and confirm the effects of ORB and GHG on the climate evolution  
112 from the MH to the PI, we conducted three additional transient experiments (Table 2). ~~Among these:-~~ Exp ORB  
113 represents the transient experiment for ORB; ~~Exp GHG represents~~, the transient experiment for GHG; ~~and Exp Full,~~  
114 ~~represents~~ the experiment where ORB, GHG, and total solar irradiance are applied concurrently. The ORB data in the  
115 transient experiments is ~~derived~~ from Berger and Loutre (1991), the GHG data is interpolated from ~~greenhouse~~  
116 ~~gas~~ GHG -data reconstructed from Antarctic ice cores, and the total solar irradiance data is ~~sourced~~ from the PMIP4

117 SATIRE-M solar forcing data (Otto-Bliesner et al., 2017). Each transient experiment starts at the MH and concludes at  
 118 the PI, spanning a total of 5900 model years. We use model years 1–500 to represent the MH climate (Stage 1), and  
 119 model years 5401–5900 to represent the PI climate (Stage 2), with and then compare the difference between Stage 1  
 120 and Stage 2 compared with the results of the equilibrium experiments (Fig. 5b). The settings for forcing information  
 121 in the transient experiments are listed in Table 2.

122

123 **Table 1. Forcings and boundary conditions in equilibrium experiments.** More details can be found in Otto-Bliesner et al.  
 124 (2017).

	Exp MH	Exp PI	Exp MH_ORB
Orbital parameters	Same as Exp MH		
Eccentricity	0.018682	0.016764	0.018682
Obliquity (degrees)	24.105	23.459	24.105
Perihelion – 180	0.87	100.33	0.87
Greenhouse gases	Same as Exp PI		
CO <sub>2</sub> (ppm)	264.4	284.3	284.3
CH <sub>4</sub> (ppb)	597	808.2	808.2
N <sub>2</sub> O (ppb)	262	273.0	273.0

125

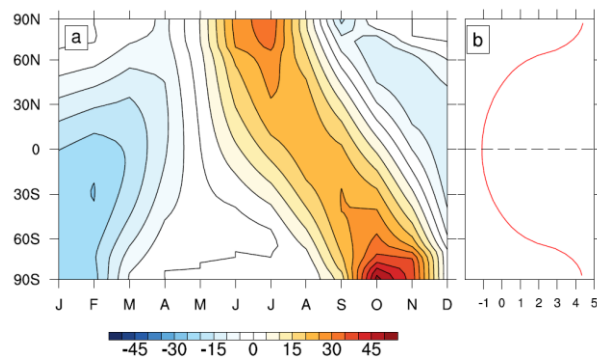
126 **Table 2. Forcings and boundary conditions in transient experiments.**

	Exp ORB	Exp GHG	Exp Full
Orbital parameters	Berger and Loutre (1991)	Same as Exp MH	Same as Exp ORB
		Flückiger et al. (2002)	
Greenhouse gases	Same as Exp MH	Monnin et al. (2004)	Same as Exp GHG
		Spahni et al. (2005)	
Total solar irradiance	Same as Exp MH	Same as Exp MH	Otto-Bliesner et al. (2017)

127

128 ORB includes Orbital parameters include eccentricity, precession, and obliquity. In the past six millennia, the  
 129 both eccentricity and obliquity did not change much. The main change came from precession, which is influenced by  
 130 eccentricity and the longitude of perihelion. As a result, perihelion is close to the NH autumn equinox in the MH  
 131 period and close to the NH winter solstice in the PI period. Therefore, with respect to Exp PI, the solar energy received  
 132 at the top of the atmosphere (TOA) in Exp MH changed seasonally and latitudinally, as shown in Fig. 1a. Compared to

133 Exp PI, Exp MH had higher NH summer radiation and lower winter radiation, and the difference during June–August  
 134 (JJA) reached  $30 \text{ W/m}^2$  in the high latitudes. Smaller precession led to more radiation received in the NH summer in  
 135 the MH period. Figure 1b shows the meridional variation of annual mean shortwave radiation at the TOA, which is  
 136 greater than  $4 \text{ W/m}^2$  poleward of  $45^\circ\text{N}$ (S), but negative and smaller than  $1 \text{ W/m}^2$  between  $45^\circ\text{S}$  and  $45^\circ\text{N}$ . This  
 137 situation is associated with the larger obliquity in the MH (Otto-Bliesner et al., 2006; Williams et al., 2020). In  
 138 addition, the difference of GHG between the MH and PI periods can lead to an effective radiative forcing of  $0.3 \text{ W/m}^2$   
 139 (Otto-Bliesner et al., 2017).



140

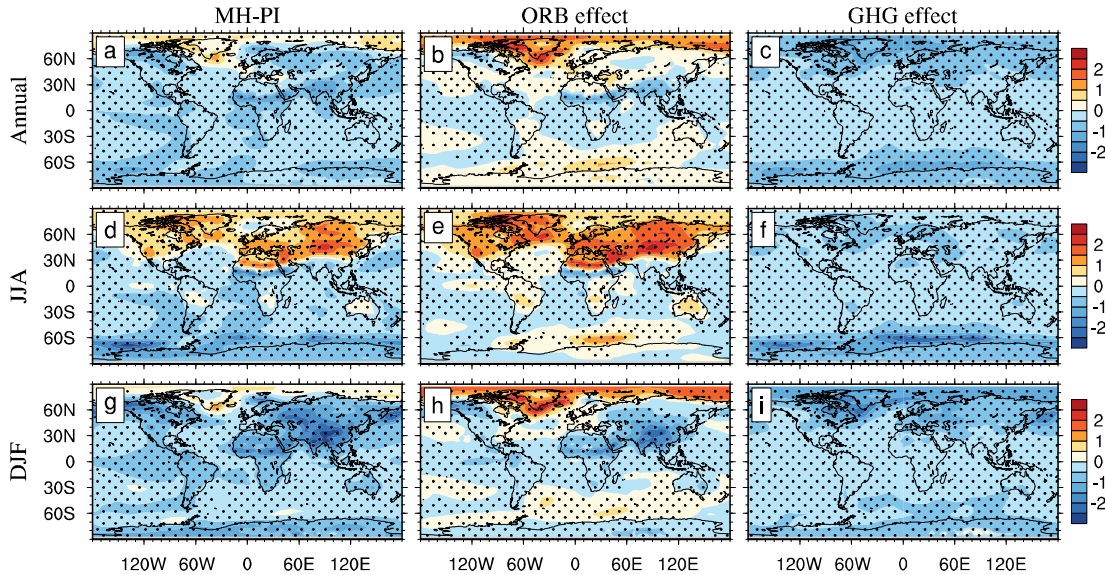
141 **Figure 1** (a) Latitude-month distribution of solar radiation change at the TOA in Exp MH, and (b) annual mean solar  
 142 radiation change, with respect to Exp PI. Units:  $\text{W/m}^2$ .

### 143 3. Results

#### 144 3.1 Surface air temperature and precipitation

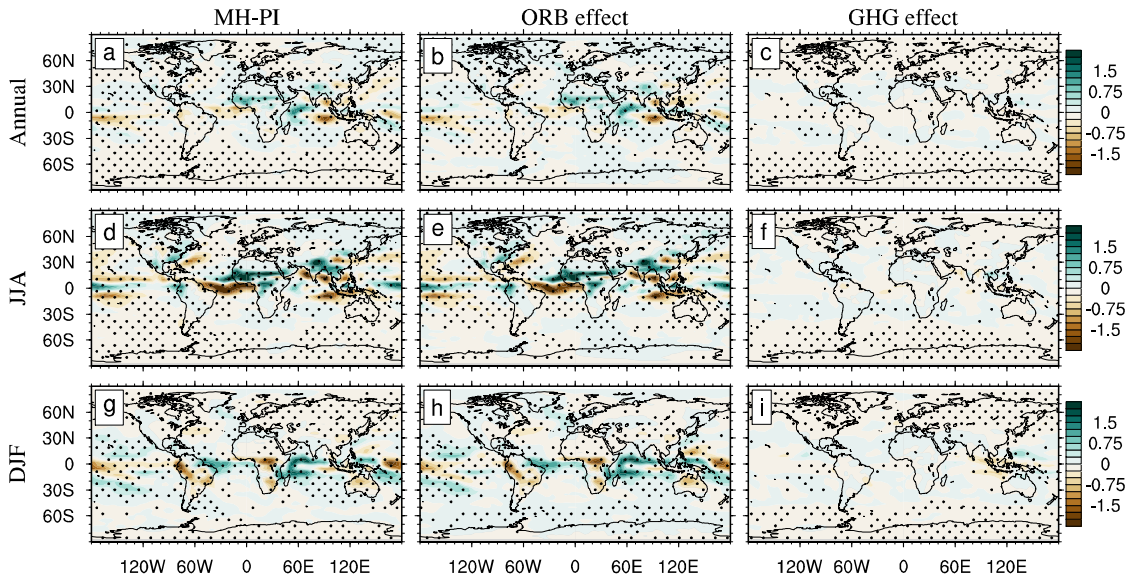
145 Compared to Exp PI, Exp MH has warmer annual mean temperatures in the NH high latitudes and cooler  
 146 temperatures in the rest of the globe (Fig. 2a), while Exp MH\_ORB has a warmer surface at mid–high latitudes in  
 147 both the NH and SH, with a greater range and magnitude than Exp MH (Fig. 2b). Figure 2b shows the direct  
 148 response to the meridional change of annual mean solar radiation. The lower GHG in the MH contributed to a lower  
 149 global surface temperature, which is clear in the mid–high latitudes (Fig. 2c). In the NH summer (June–August, or  
 150 JJA), Exp MH shows a general warming of more than  $1^\circ\text{C}$  north of  $30^\circ\text{N}$ , which is more significant in Greenland and  
 151 Euro-Asian continent, and a cooling belt in northern India and central Africa (Fig. 2d), which is associated with  
 152 increased rainfall due to the enhanced monsoon (Fig. 2d). The magnitude and extent of warming due to the ORB effect  
 153 are apparently greater, with warming of up to  $3^\circ\text{C}$  in central Asia (Fig. 2e). The GHG cooling is more pronounced  
 154 over the Southern Ocean (Fig. 2f). In the NH winter (December–February, or DJF), only the NH polar latitudes  
 155 remain the warming. There is strong cooling (up to  $3^\circ\text{C}$ ) in the African and Euro-Asian continents (Fig. 2g). The  
 156 patterns under the ORB and GHG forcing are similar to their annual mean situations, except for the enhanced cooling

157 in South Asia and central Africa (Fig. 22h) and over the subpolar Atlantic (Fig. 22i). Most figures ~~are featured with~~  
 158 ~~ashow~~ polar amplification, which may be related to the change of sea ice (Otto-Bliesner et al., 2017; Williams et al.,  
 159 2020).



160  
 161 **Figure 22** (Left column) Changes in SAT in ~~the~~-Exp MH, with respect to ~~the~~-Exp PI, and the contributions from (central  
 162 column) the ORB effect and (right column) the GHG effect. (a)–(c) are for annual mean; (d)–(f), for ~~the~~-NH JJA; and (g)–  
 163 (i), for ~~the~~-NH DJF. Stippling shows significance over the 90% level calculated by Student *t*-test. Units: °C.

164  
 165 Differences in precipitation between the MH and PI simulations are shown in Fig. 33. Consistent with the  
 166 latitudinal and seasonal differences of insolation (Fig. 1), the largest difference in precipitation between the two  
 167 periods also occurs in the NH summer, with significantly more precipitation in northern India and ~~in the~~ equatorial  
 168 African monsoon region, and drier in the equatorial Atlantic and Pacific in Exp MH (Fig. 33d). The difference  
 169 between Exps MH and PI is mainly in the global tropics, and is contributed predominantly by the ORB effect (Figs.  
 170 33e, h), as the GHG effect is very weak (Figs. 33f, i).



171

172

**Figure 33** Same as Fig. 22, but for precipitation change. Units: mm/day.

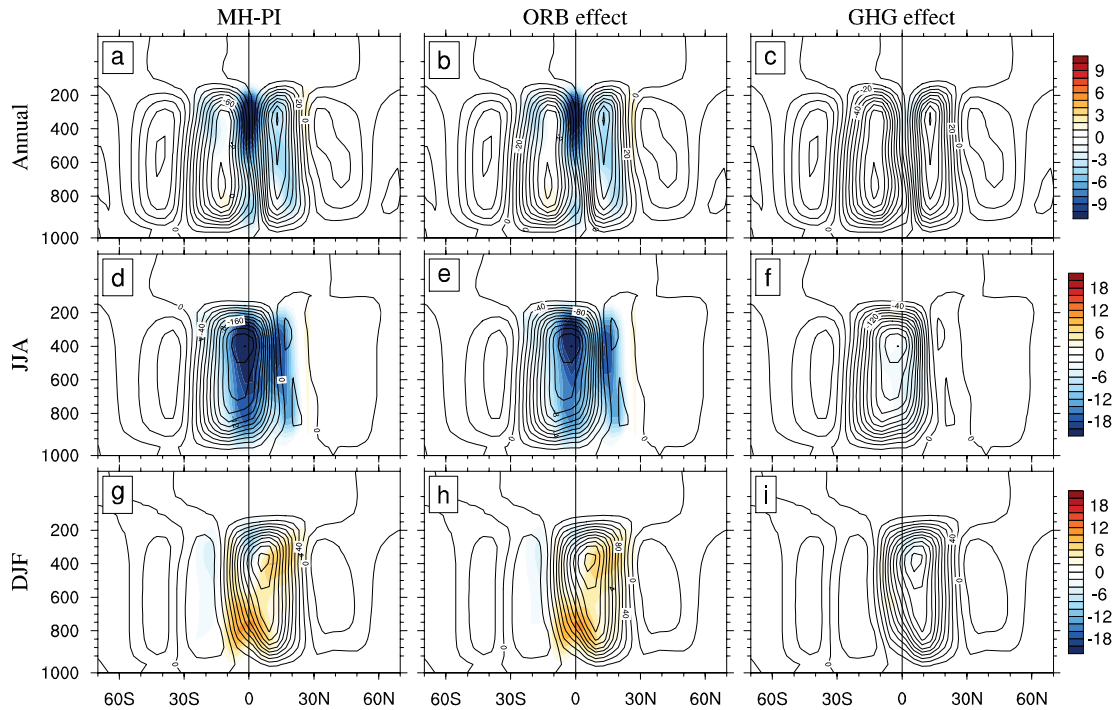
173

174 Although the numerical values may be slightly different due to different models or resolutions, in general the  
 175 annual and seasonal climatology differences of temperature and precipitation between Exps MH and PI are in good  
 176 agreement in some according to recent studies (Williams et al., 2020; Zhang et al., 2021b). The ORB effect dominates  
 177 the changes in global surface temperature and precipitation. Thus, Exp MH has a warmer climate than Exp PI,  
 178 particularly in the NH high latitudes.

179

180 **3.2 Meridional atmospheric circulation**

181 The meridional atmospheric circulation, namely, the Hadley cell, in Exp MH is about 10% weaker than that in  
 182 Exp PI (Fig. 44a), consistent with the weaker meridional atmospheric temperature gradient in Exp MH than in Exp PI.  
 183 The weaker Hadley cell in Exp MH is mainly due to the ORB effect (Figs. 44b, e, h). The GHG effect can be  
 184 neglected (Figs. 44c, f, i). The Hadley cell is weaker due to the strong warming of the high-latitude temperatures in the  
 185 NH summer (Fig. 44d). The strengthening of the Hadley cell in the NH winter (Fig. 44g) corresponds to an increasing  
 186 temperature gradient between the tropics and mid latitudes (Fig. 22g). The weaker Hadley cell also leads to a weaker  
 187 meridional atmospheric heat transport from low to high latitudes, which will be discussed in section 3.4.



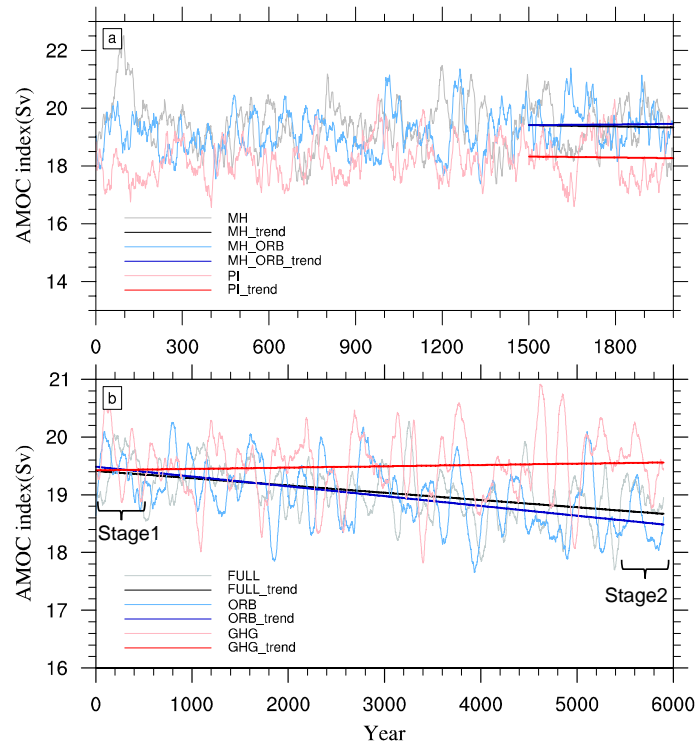
188

189 **Figure 44** Same as Fig. 22, but for the mean Hadley cell in Exp PI (contour) and its changes (shading) in Exp MH. Units:  
190  $10^9 \text{ kg/s}$ .

191

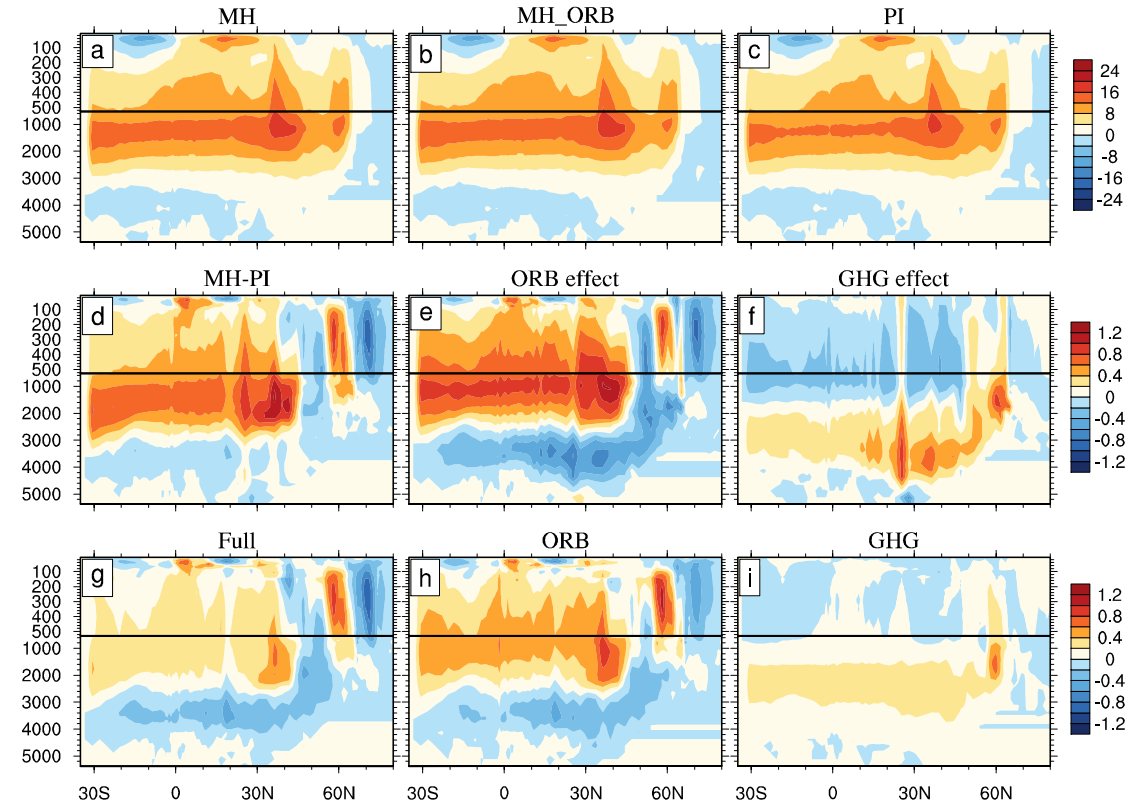
### 192 **3.3 Atlantic meridional overturning MOC circulation**

193 The AMOC strength, defined as the maximum streamfunction between 0 and  $-2000 \text{ m}$  and between  $20^\circ$  and  $-70^\circ \text{N}$  in the North Atlantic, are 19.4 and 18.3 Sv in Exps MH and PI, respectively. Figure 5a shows the time series of  
194 the AMOC of the three equilibrium experiments, all of which reached the equilibrium state. The AMOC in Exp  
195 MH\_ORB (dark blue solid line) is 1 Sv stronger than that in Exp PI (dark red solid line), while the AMOC in Exp MH  
196 (dark black solid line) is roughly the same as that in Exp MH\_ORB. Figure 5b shows the evolution of the AMOC in  
197 the three transient experiments. In Exp ORB, the AMOC strength shows a downward trend (dark blue line). In Exp  
198 GHG, the AMOC strength exhibits a slight increase with an indistinct trend (dark red line). In Exp Full, the trend of  
199 AMOC strength is essentially between Exps ORB and GHG, indicating a combined effect of external forcing factors  
200 (dark black line).



202  
 203 **Figure 5** (a) Evolutions of the AMOC in Exp MH (gray and black lines), Exp MH ORB (blue lines), and Exp PI (red lines).  
 204 (b) Evolutions of the AMOC in Exp Full (gray and black lines), Exp ORB (blue lines), and Exp GHG (red lines). The  
 205 **darkthick** lines indicate the linear trends of the AMOC in different experiments. Units: Sv (1 Sv= $10^6$  m $^3$ /s).

206  
 207 The patterns of the AMOC are shown in Fig. 6. The depth of the maximum AMOC in all experiments occurs  
 208 near 1000 m. The AMOC patterns in Exps MH and PI are similar (Figs. 6a, c), which suggests that the combined  
 209 effect of the ORB and GHG on the AMOC is small (Fig. 6d). This is similar to some recent studies, even though there  
 210 are slight differences north of 45°N (Brierley et al., 2020; Williams et al., 2020). However, individual effects of the  
 211 ORB and GHG are not negligible (Figs. 4e, f). In fact, the ORB effect leads to 6% stronger AMOC in Exp MH than  
 212 in Exp PI (Fig. 5e). The deep overturning is significantly enhanced south of 45°N, but slightly weakened north of  
 213 45°N. However, at the same time the GHG effect leads to a slight decline in AMOC strength in Exp MH, especially  
 214 above 1500 m south of 45°N (Fig. 5f). The ORB and GHG have the opposite effects on the AMOC, which make the  
 215 AMOC in Exp MH roughly the same as that in Exp PI. This is different from most previous findings (Otto Bliesner et  
 216 al., 2006; Shi and Lohmann, 2016). Figure 6(g-i, h, i) further shows the effects of different forcing factors on the  
 217 AMOC patterns in the transient experiments, which are. It can be seen that this is similar to the changes in the  
 218 equilibrium experiments (Figs. 6d-f), although there are differences in intensity, which may be due to the  
 219 influence of other external forcings. The offsetting effect between different ORB and GHG in the transient  
 220 experiments forcings is the same as that in the equilibrium experiments obvious.



221

222 **Figure 65** Patterns of mean AMOC in (a) Exp MH, (b) Exp MH\_ORB, and (c) Exp PI; and (d) the AMOC change in Exp  
 223 MH, with respect to Exp PI. (e) and (f) show the AMOC changes due to the ORB effect and GHG effect, respectively. (g),  
 224 (h), (i) represent the AMOC changes between of the two stages AMOC (Sstage1-Sstage2) in the Exps Full, ORB, and GHG,  
 225 respectively. The AMOC index is defined as the maximum streamfunction in the range of 0–2000 m of 20°–70°N in the  
 226 North Atlantic. Units: Sv (1 Sv =  $10^6 \text{ m}^3/\text{s}$ ).

227

228

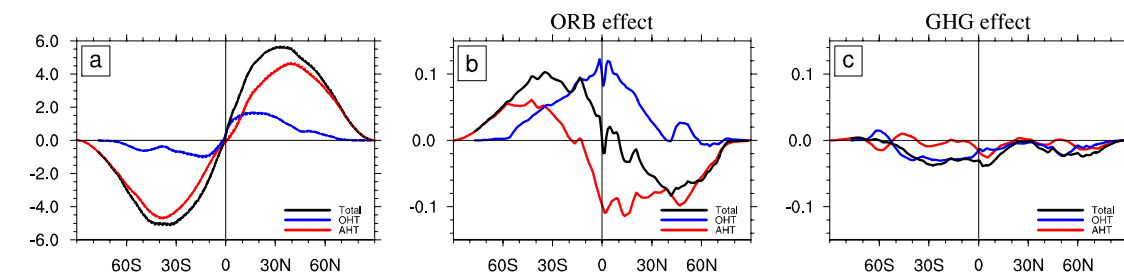
### 229 3.4 Meridional heat transport

230 Meridional heat transport (MHT) plays an important role in maintaining energy balance of the Earth climate  
 231 system. Figure 67a shows the annual MHTs in different experiments, which are nearly identical. The climate  
 232 differences between Exps MH and PI hardly change the integrated heat transport in both the atmosphere and ocean.  
 233 Consistent with previous studies (Trenberth and Caron, 2001), the annual mean MHT shows an antisymmetric  
 234 structure about the equator, with the peak value of about 5.5 PW (1 PW =  $10^{15} \text{ W}$ ) at 40°N/S. Compared with ocean  
 235 heat transport (OHT), the atmosphere heat transport (AHT) dominates at most latitudes, which is also consistent with  
 236 most previous studies (Held, 2001; Wunsch, 2005; Czaja and Marshall, 2006).

237 However, the MHT changes caused by the ORB and GHG effects appear to be nonnegligible. The ORB causes  
 238 an increase in OHT in the NH, with the maximum change of about 0.10 PW near the equator, roughly 10% of the

239 mean OHT there. This is due to the enhanced AMOC, and is the main cause of temperature increase in the NH high  
 240 latitudes (Fig. 2b). The northward AHT is reduced, with the maximum change of about 0.10 PW. This is due to the  
 241 weakened Hadley cell. The AHT change compensates the OHT change very well in the deep tropics, while the former  
 242 overcompensates the latter in the NH off-equatorial regions (Fig. 67b). The GHG effect on the MHT is very weak, with  
 243 the maximum MHT change of no more than 0.04 PW near 5°N (Fig. 7c), which is just one third of the ORB-induced  
 244 MHT change (Fig. 67eb).

245



246

247 **Figure 67** (a) Annual mean meridional heat transport (MHT). Black, red, and blue lines are for the total MHT, AHT, and  
 248 OHT, respectively. Solid, dashed, and dotted lines are for Exps MH, MH\_ORB, and PI, respectively. (b) and (c) show  
 249 changes in the total MHT, AHT, and OHT due to ORB and GHG effects, respectively. Units: PW (1 PW =  $10^{15}$  W).

250

251

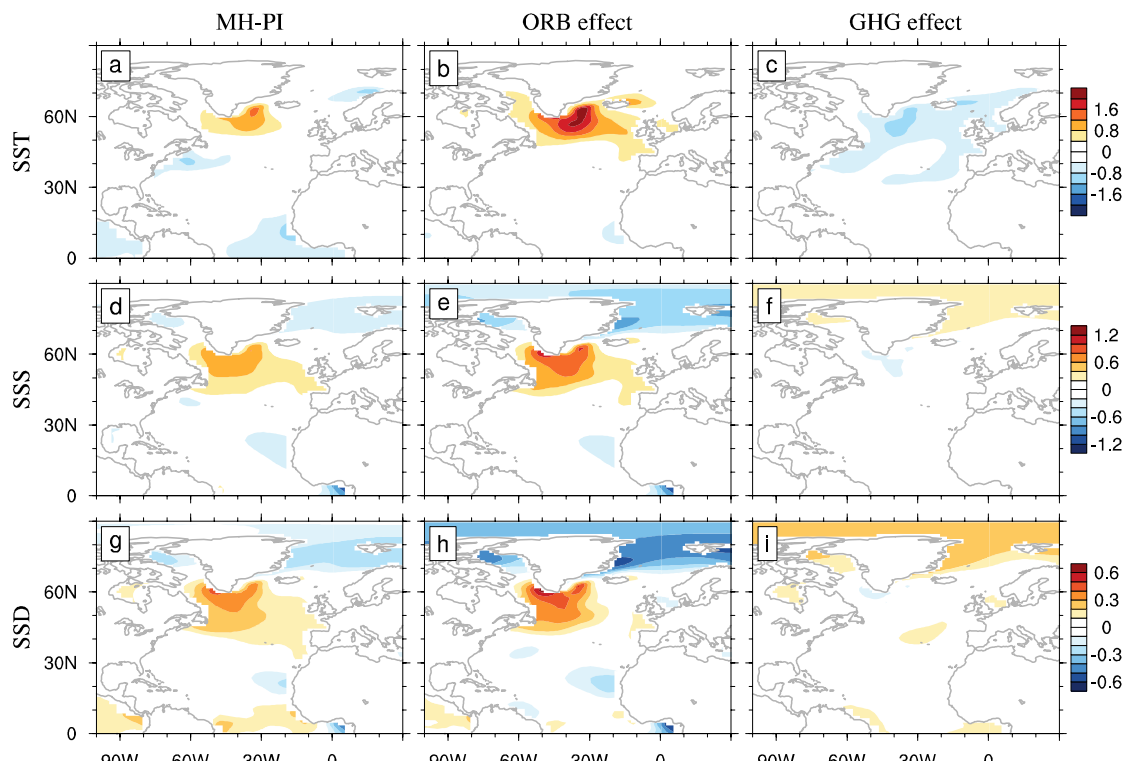
#### 252 4. Changes in the North Atlantic Ocean

##### 253 4.1 Changes in sea-surface temperature, salinity, and density

254 The strength of the AMOC is largely determined by the North Atlantic deep-water formation, which is in turn  
 255 determined by upper-ocean density. Figures 78 and 9 shows the differences of sea-surface temperature (SST), salinity  
 256 (SSS), and density (SSD) in the North Atlantic between Exps MH and PI, and the two stages in the transient  
 257 experiments, respectively. The SST difference is characterized by a warming up to 1.6°C in the subpolar Atlantic and a  
 258 cooling of about 1°C near the Nordic Seas and Gulf Stream extension region (Fig. 78a). The surface ocean warming in  
 259 the North Atlantic is due to the ORB effect (Fig. 78b), which causes a strong and extensive warming in the North  
 260 Atlantic, with the maximum warming in the subpolar Atlantic. The GHG effect causes a general cooling in the North  
 261 Atlantic (Fig. 78c), offsetting partially the ORB-induced warming, leaving a cooling in the Nordic Seas and Gulf  
 262 Stream extension (Fig. 78a). The North Atlantic main area of SST changed difference in the North Atlantic of Exp Full  
 263 (Fig. 9a) is consistent with that of Exp MH (Fig. 8a), although the magnitude is slightly lowersmaller(Fig. 9a), Exp

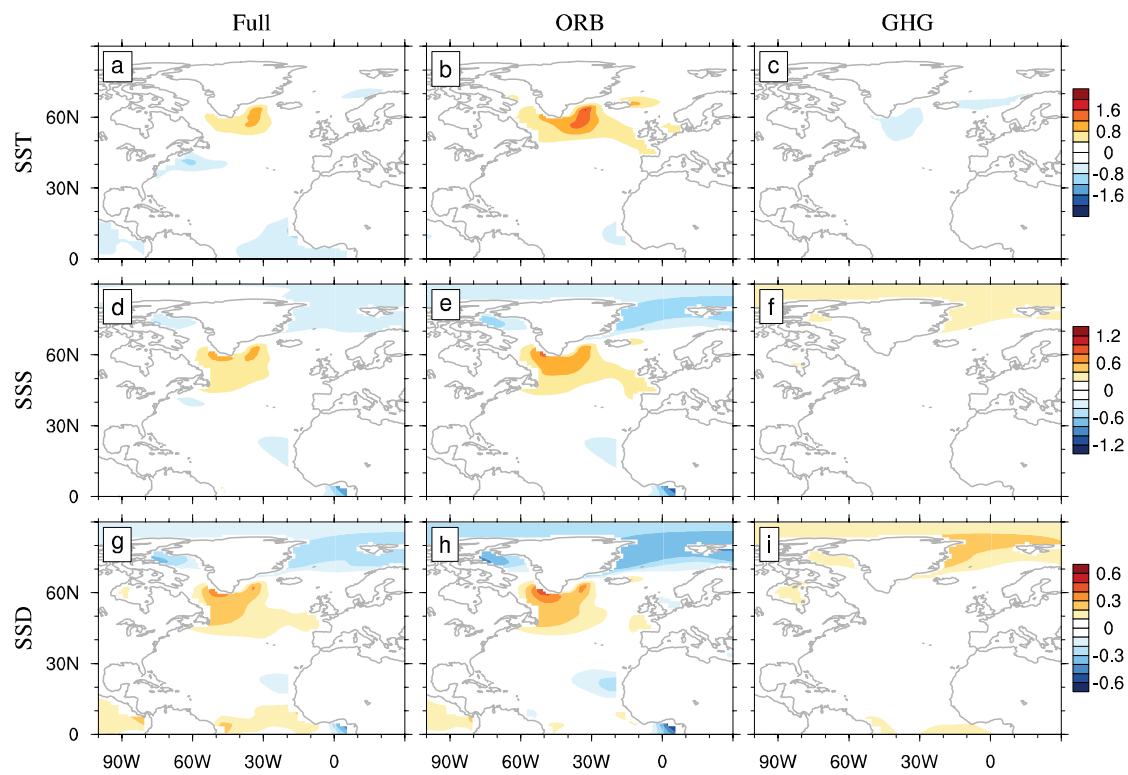
264 ORB also exhibits stronger warming than Exp Full (Fig. 9b), consistent with Fig. 8b, and Exp GHG also shows  
 265 a slight cooling offsets part of the warming (Figs. 9b, c), consistent with Fig. 8c. Overall, the SST change in of the  
 266 transient experiments is almost the same as that of in the equilibrium experiments, although not as much in  
 267 magnitude.

268 The patterns of SSS difference between Exps MH and PI are similar to those of SST difference. In general, the  
 269 North Atlantic is more saline in Exp MH than in Exp PI (Fig. 78d), mainly due to stronger evaporation over  
 270 precipitation in Exp MH than in Exp PI (Fig. 912d), which is in turn due to the warmer SST forced by the ORB effect  
 271 (Fig. 78e). The polar oceans are fresher in Exp MH than in Exp PI (Figs. 78d, e), mainly due to more freshwater flux  
 272 coming from ~~the~~ sea ice in Exp MH (Figs. 912a, b), consistent with the warmer climate in the MH due to the ORB  
 273 effect. The SSS difference caused by the GHG effect is roughly opposite to that caused by the ORB effect, but with  
 274 much weaker magnitude (Fig. 78f), because the cooling effect of the GHG makes less evaporation in the subtropical  
 275 to subpolar Atlantic and more sea ice in the polar oceans (Fig. 912c). Similar to the equilibrium experiments, the SSS  
 276 changes in SSS of the transient experiments also showed the similar characteristics (Figs. 9d, e, f). Exp ORB caused a  
 277 significant increase in SSS, reaching 0.6 psu, while the effect of GHG was not obvious (Figs 9e, f).



278  
 279 **Figure 78** Changes in (a)–(c) sea-surface temperature (SST), (d)–(f) sea-surface salinity (SSS), and (g)–(i) sea-surface  
 280 density (SSD) of the North Atlantic in Exp MH, with respect to ~~the~~ Exp PI. (a), (d), and (g) are for the total changes; (b), (e),  
 281 and (h), for the changes due to ORB effect; (c), (f), and (i), are for changes due to GHG effect. Units are  $^{\circ}\text{C}$  for SST, psu  
 282 for SSS, and  $\text{kg}/\text{m}^3$  for SSD.

283  
 284 The patterns of SSD difference (Figs. 8g–i) resemble those of both SSS and SST differences, while its polarity is  
 285 determined by SSS difference. The higher SSD in the North Atlantic is favorable for a stronger deep-water formation  
 286 and thus a stronger AMOC in Exp MH. Forced by the ORB effect, the North Atlantic surface ocean can be  $0.5 \text{ kg/m}^3$   
 287 denser in Exp MH than in Exp PI (Fig. 8h), which could have resulted in a 1.2-Sv stronger AMOC in Exp MH than in  
 288 Exp PI (Fig. 6e). However, the GHG effect, although weak, has an opposite effect on SSD and thus the AMOC (Fig.  
 289 8i), and eventually mitigates the ocean change in Exp MH. ~~S~~The similar patterns of SSD are shown in the transient  
 290 experiments, with increased North Atlantic density in Exp ORB, and the opposite and weaker effect in Exp GHG  
 291 (Figs. 9g, h, i), corresponding to changes in the AMOC (Fig. 6). These suggest that the mechanisms of ORB and GHG  
 292 on the climate change in the equilibrium and transient experiments are consistent.



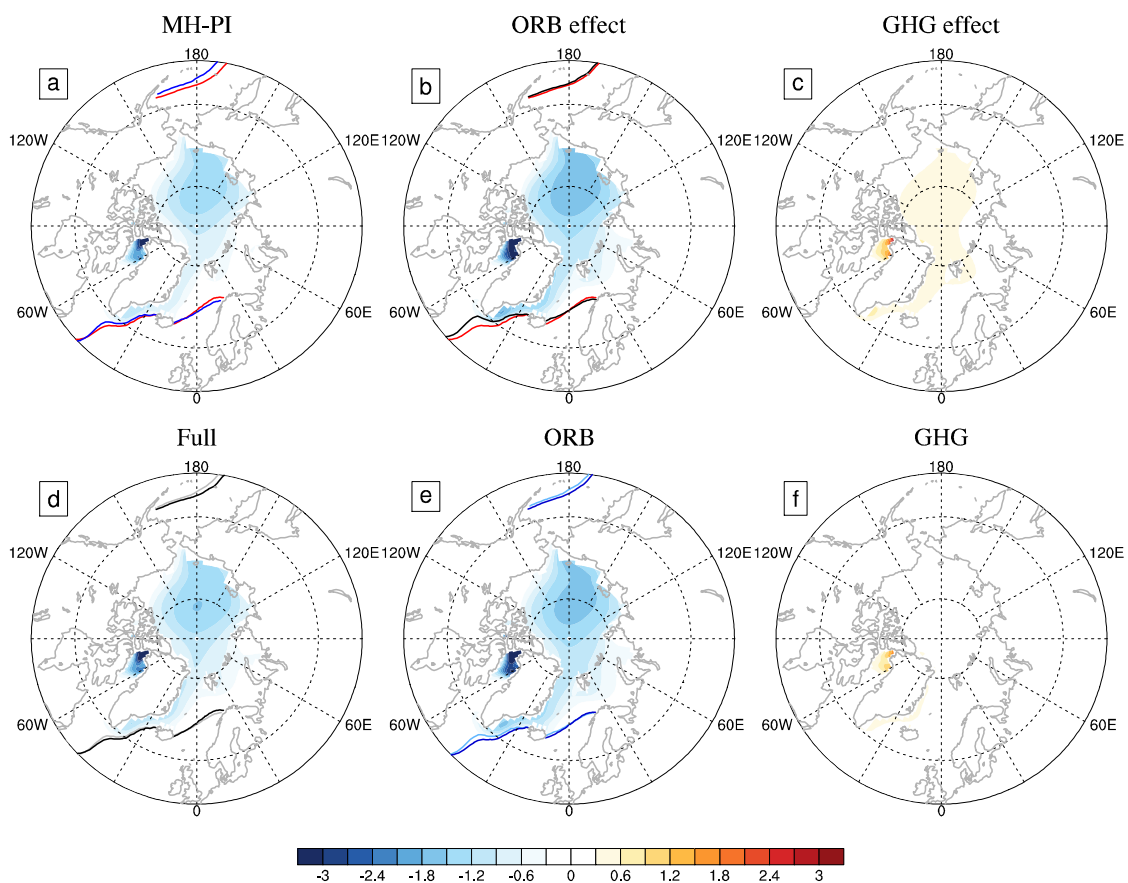
294  
 295 **Figure 9** Similar to Fig. 8, but for Exps Full, ORB, and GHG, respectively. All variables are represented as changes  
 296 between the in two stages (Sstage1-Sstage2).

297

298 **4.2 Change in surface freshwater flux**

299 Sea-surface freshwater flux includes both sea-ice formation (melting) and net evaporation (i.e., evaporation  
 300 minus precipitation, or EMP). Figure 810 shows the change of annual mean sea-ice thickness in the Arctic. The Arctic

301 sea-ice thickness in Exp MH is about 1.0 m thinner than that in Exp PI (Fig. 810a). The largest sea-ice difference,  
 302 which is about 3.0 m thinner in Exp MH, occurs in the Baffin Bay. When forced by the ORB effect only, the Arctic  
 303 sea-ice [no “-“] would be more than 1.5 m thinner (Fig. 810b), consistent with the stronger insolation and the  
 304 warming in the NH high latitudes (Figs. 1, 2e). The GHG effect leads to a slight increase of sea ice in the Arctic (Fig.  
 305 810c) in Exp MH, which is less than 0.5 m in thickness. Changes in Arctic sea-ice thickness can affect sea-ice  
 306 transport to the subpolar Atlantic. The loss of sea ice in the central Arctic Ocean can reduce its export through the  
 307 Fram Strait, which can lead to an increase in salinity in the associated subpolar [no “-“] regions (Shi and Lohmann,  
 308 2016), as shown in Figs. 78d and e. Similar changes in sea-ice thickness also occur in the transient experiments; with  
 309 Exp ORB leading to a decrease in the Arctic sea-ice thickness is decreased significantly in Exp ORB, while it is nearly  
 310 unchanged and a weak change in Exp GHG- (Figs. 10e, f1b, e), reflecting the consistency of the effects of ORB and  
 311 GHG in the both equilibrium and transient experiments.



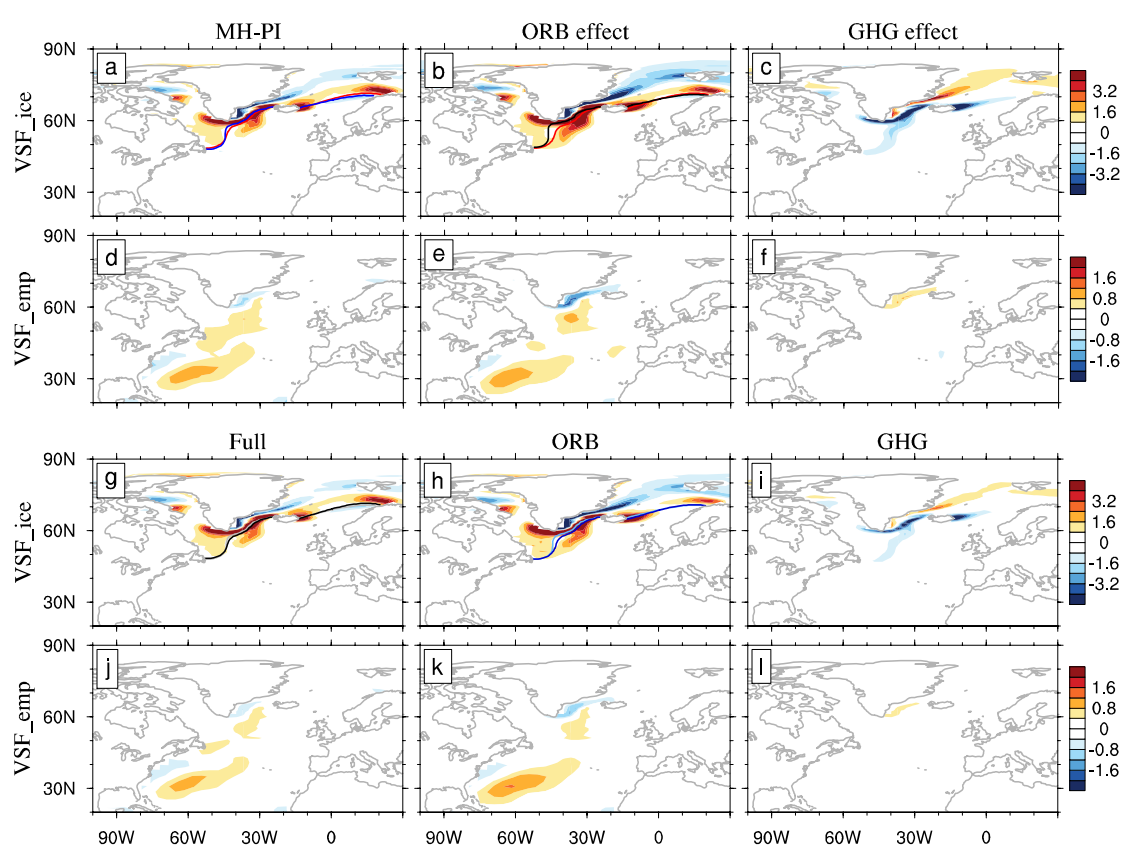
313 **Figure 108** (a)-(c) Changes in the Arctic mean sea-ice thickness in Exp MH, with respect to Exp PI. Positive (negative)  
 314 value represents sea-ice formation (melting). (a) is for the total change; (b) and (c), for changes due to ORB and GHG  
 315 effects, respectively. Solid blue, black, and red curves show the sea-ice margin in Exps MH, MH\_ORB and PI, respectively.  
 316 (d)-(f) Same as (a)-(c), except for Exps Full, ORB, and GHG, respectively. The solid gray and light blue curves indicate  
 317 the sea-ice margin of Stage1 in the Exps Full and ORB, respectively; and the black and dark blue solid curves represent the

318 sea-ice margin of Stage2 in the Exps Full and ORB, respectively. The sea-ice margin is defined by the 15% sea-ice fraction.  
319 Units: m.

320

321 The sea-ice margin in the North Atlantic in Exp MH is slightly more northward compared to that in Exp PI (solid  
322 blue curve, Fig. 8121a). The curves in Fig. 8112 show sea-ice margin in different experiments. The northward  
323 displacement of sea-ice margin and the decrease in sea-ice volume in the Arctic favor the decrease in freshwater flux  
324 in the North Atlantic, helping a more saline North Atlantic, which contributes about 0.9 psu 10yr<sup>-1</sup> to the SSS tendency  
325 between 40° and 60°N (Fig. 9112a). The EMP flux is small, and the upper ocean is refreshed at a steady rate of about  
326 0.09 psu 10 yr<sup>-1</sup> in the North Atlantic (Fig. 9121d). The contributions of sea-ice change and EMP flux contributions to  
327 SSS in the transient experiments are also about 0.9 and 0.09 psu 10 yr<sup>-1</sup>, respectively (Figs. 131ga, dj). Overall, for the  
328 North Atlantic the change of sea ice plays a dominant role; and its contribution to SSS tendency is about 10 times that  
329 of EMP.

330



331  
332 **Figure 1129** Changes in (a)–(c) are, namely, virtual salt flux (VSF) due to sea ice, and in (d)–(f), VSF due to EMP in Exp  
333 MH, with respect to Exp PI. Positive (negative) value represents sea-ice formation (melting) or evaporation larger (smaller)  
334 than precipitation. (a) and (d) are for total changes; (b) and (e) are for changes due to ORB effect; (c) and (f) are for GHG

335 effect. (g)–(l) Same as (a)–(f), but for Exp Full, Exp ORB, and Exp GHG, respectively. The solid gray and light blue  
336 curves indicate the sea-ice margin of Stage1 in the Exps Full and ORB, respectively; and the black and dark blue solid  
337 curves represent the sea-ice margin of Stage2 in the Exps Full and ORB, respectively. The sea-ice margin in (a)–(b) are is  
338 defined the same way as those that in Fig. 8. Units: psu 10 yr<sup>-1</sup>.

339

340 The sea-ice margin in Exp MH is controlled by the ORB effect. In individual forcing experiment, the sea-ice  
341 margin forced by the ORB effect is almost the same as that in Exp MH (solid black curve, Fig. 9112b). The  
342 contributions of ORB and GHG effects to changes in virtual salt flux (VSF) due to sea ice are 1.3 and -0.4 psu 10 yr<sup>-1</sup>,  
343 respectively (Figs. 9112b, c); and those due to the EMP flux are 0.06 and 0.03 psu 10 yr<sup>-1</sup>, respectively (Figs. 9112e,  
344 f). and in the transient experiments, the contributions of ORB and GHG effects to the VSF due to sea ice are 1.1 and  
345 -0.2 psu 10 yr<sup>-1</sup>, respectively (Figs. 113bh, ie); and those due to EMP flux are 0.05 and 0.03 psu 10 yr<sup>-1</sup>, respectively  
346 (Figs. 131ei, lf). This suggests that the sea-ice change caused by the ORB effect plays an important role in the  
347 enhancement of the AMOC in Exp MH.

348 In general, the modelling results suggest that the stronger AMOC in Exp the MH period is resulted from more  
349 saline North Atlantic, which was contributed mainly by smaller freshwater flux coming from the Arctic. The  
350 contribution of EMP to salinity change was small, which was only one-tenth of the sea-ice contribution. ORB and  
351 GHG consistently play opposite roles in the deep-water formation of the subpolar Atlantic. Their combined effect  
352 resulted in little change in the AMOC in Exp the MH period, which is less than with only about 0.81 Sv enhancement  
353 in both the equilibrium and transient experiments. The results are further validated by a series of results from transient  
354 experiments, albeit with slight differences in magnitude, which may be due to the simultaneous application of TSI to  
355 the Exp Full. However, the offsetting effects of ORB and GHG are very clear.

356

## 357 5. Summary and discussion

358 In this study, three-six experiments using the CESM1.0 were conducted to quantify the contributions of ORB and  
359 GHG effects to the MH climate. Most attention was paid to the AMOC; and the mechanism to the insignificant  
360 difference of the AMOC between the MH and PI periods was explored. This study is the first attempt to separate the  
361 ORB and GHG effects on the MH climate. Simulations showed that the NH climate exhibits much greater regional  
362 and seasonal variability due to the seasonal enhancement of insolation caused by changes in ORB; and these  
363 contrasting seasonal responses lead to little change in annual mean climate (Fig. 23b). Lower GHG in Exp MH has a

364 global cooling effect, with greater temperature decreases at higher latitudes associated with feedbacks from sea ice and  
365 snow cover (Fig. 23e). The combined effect of these two forcing factors leads to a weak warming at the NH high  
366 latitudes and cooling elsewhere (Fig. 23a), similar to the temperature changes in the PMIP4 ensemble (Brierley et al.,  
367 2020).

368 Weakening meridional atmospheric temperature gradient in Exp MH leads to the Hadley cell being weakened by  
369 about 10% in the NH (Fig. 44a). At the same time, due to the change of sea-surface buoyancy in the North Atlantic,  
370 the AMOC is slightly enhanced by about 4% (Fig. 56a). As far as the changes in MHT magnitude in the NH are  
371 concerned, the effect of ORB is about five times that of GHG (Figs. 67b, c). Our experiments also showed that the  
372 change in the AMOC is mostly determined by the freshwater flux change in the North Atlantic, which is in turn  
373 closely related to the Arctic sea-ice change related to the ORB effect. GHG has the opposite effect to ORB, which  
374 mitigates the enhancement of the AMOC (Figs. 9b, c). long term transient experiments further prove the mutual  
375 cancelation of external forcings (Figs. 6h, i).

376 The conclusions drawn in this paper may be model-dependent. Shi and Lohmann (2016) simulated a stronger  
377 MH AMOC in the high-resolution version of the ECHAM, with a maximum change of more than 2 Sv. Most of the  
378 models in the CMIP5 reveal a positive AMOC change in the MH period. Some previous studies (Ganopolski et al.,  
379 1998; Otto-Bliesner et al., 2006) showed that the AMOC in the MH is weaker than that of the PI period. The main  
380 reason for the inconsistency is that the simulated ocean salinity in the North Atlantic is different. Therefore, it is  
381 necessary to carry out simulations with multiple models to reduce model dependence. In addition to the model itself,  
382 whether the experimental setting includes the GHG is also an important factor. Our results simulations on the AMOC  
383 in the MH are similar to those of (Jiang et al., 2023), but our focus is to find the mutual offsetting effect between  
384 external forcing factors. The experiments we conducted are time slice experiments. And it is necessary to study  
385 whether the offsetting effects of the ORB and GHG exists in transient experiments, both showing no significant  
386 changes in the AMOC in the MH compared with the PI; however, their study did not explain the mechanism behind  
387 this phenomenon. Our study reveals the competitive relationship between the two forcing factors through multiple-  
388 equilibrium state simulations and transient simulations, which is a significant advancement. It supports the  
389 popular existing conclusions about the AMOC change from in the MH to the PI periods and sheds light on the  
390 mechanisms underlying the small differences simulated during MH.

391 Our experiments study focuses on only considering the effects of ORB and GHG effects; and the simulated cooler  
392 annual mean temperature over in most areas of the NH differs from the warming record revealed by most proxy data  
393 (Wanner et al., 2008; Larrosoana, 2012; Liu et al., 2014), but is similar to the conclusions from the PMIP4

394 simulations. It is unclear whether these differences originate from the model, the data record, or a combination of  
395 ~~both the two~~. Some proxy data suggested that the climate of North Africa was wetter in the MH period, which was  
396 known as the Green Sahara. ~~(Jiang et al., 2012) analyzed six sets of PMIP2 coupled models' results, and found that~~  
397 ~~the dynamic vegetation has little impact on regional climate. Jiang et al. (2012) analyzed the simulation results of six~~  
398 ~~coupled models in PMIP2 for the mid-Holocene MH period. They found that the dynamic vegetation effect led to a~~  
399 ~~decrease in annual cooling over China in five of these models during the MH is period, although its impact on the mid-~~  
400 ~~Holocene MH temperature was minimal.~~ Braconnot et al. (2021) and Zhang et al. (2021a) studied the effect of dust  
401 reduction on climate due to the greening of the Sahara desert, using the CESM and IPSL models, respectively,  
402 showing global mean surface temperature increased by about  $0.1^{\circ}\text{C}$ . Although there are other forcing factors in the  
403 MH period, such as vegetation, dust, and topography, overall our simulations are representative of the most important  
404 forcing factors and provide quantified estimates of the contributions of ORB and GHG effects ~~onto~~ the MH climate.  
405

406 **Acknowledgements.** This work is supported by the National Natural Science Foundation of China (Nos. 42230403,  
407 42288101, ~~and~~ 41725021) and by the foundation at the Shanghai Frontiers Science Centre of Atmosphere-Ocean  
408 Interaction of Fudan University. The experiments were performed on the supercomputers at the Chinese National  
409 Supercomputer Centre in Tianjin (Tian-He No.1).  
410

411 **References**

412 Berger, A. and Loutre, M. F.: Insolation values for the climate of the last 10 million years, Quaternary Sci. Rev., 10,  
413 297-317, [https://doi.org/10.1016/0277-3791\(91\)90033-Q](https://doi.org/10.1016/0277-3791(91)90033-Q), 1991.

414 Braconnot, P., Albani, S., Balkanski, Y., Cozic, A., Kageyama, M., Sima, A., Marti, O., and Peterschmitt, J. Y.:  
415 Impact of dust in PMIP-CMIP6 mid-Holocene simulations with the IPSL model, Clim. Past, 17, 1091-1117,  
416 <http://doi.org/10.5194/cp-17-1091-2021>, 2021.

417 Brierley, C. M., Zhao, A., Harrison, S. P., Braconnot, P., Williams, C. J. R., Thornalley, D. J. R., Shi, X., Peterschmitt,  
418 J.-Y., Ohgaito, R., Kaufman, D. S., Kageyama, M., Hargreaves, J. C., Erb, M. P., Emile-Geay, J., D'Agostino, R.,  
419 Chandan, D., Carré, M., Bartlein, P. J., Zheng, W., Zhang, Z., Zhang, Q., Yang, H., Volodin, E. M., Tomas, R.  
420 A., Routson, C., Peltier, W. R., Otto-Bliesner, B., Morozova, P. A., McKay, N. P., Lohmann, G., Legrande, A.  
421 N., Guo, C., Cao, J., Brady, E., Annan, J. D., and Abe-Ouchi, A.: Large-scale features and evaluation of the  
422 PMIP4-CMIP6 &lt;i&gt;midHolocene&lt;/i&gt; simulations, Clim. Past, 16, 1847-1872,  
423 <https://doi.org/10.5194/cp-16-1847-2020>, 2020.

424 Brown, N. and Galbraith, E. D.: Hosed vs. unhosed: interruptions of the Atlantic Meridional Overturning Circulation  
425 in a global coupled model, with and without freshwater forcing, Clim. Past, 12, 1663-1679,  
426 <https://doi.org/10.5194/cp-12-1663-2016>, 2016.

427 Chen, C.-T. A., Lan, H.-C., Lou, J.-Y., and Chen, Y.-C.: The Dry Holocene Megathermal in Inner Mongolia,  
428 Palaeogeogr. Palaeoclimatol. Palaeoecol., 193, 181-200, [https://doi.org/10.1016/s0031-0182\(03\)00225-6](https://doi.org/10.1016/s0031-0182(03)00225-6), 2003.

429 Czaja, A. and Marshall, J.: The Partitioning of Poleward Heat Transport between the Atmosphere and Ocean, Global  
430 Planet. Change., 63, 1498-1511, <https://doi.org/10.1175/jas3695.1>, 2006.

431 [Fox-Kemper, B., H.T. Hewitt, C. Xiao, G. Aðalgeirsdóttir, S.S. Drijfhout, T.L. Edwards, N.R. Golledge, M. Hemer, R.E. Kopp, G. Krinner, A. Mix, D. Notz, S. Nowicki, I.S. Nurhati, L. Ruiz, J.-B. Sallée, A.B.A. Slangen, and Y. Yu: Ocean, cryosphere and sea level change. In V. Masson-Delmotte, P. Zhai, A. Pirani, S. L. Connors, C. Péan, S. Berger, et al. \(Eds.\), Climate change 2021: The physical science basis. Contribution of working group I to the sixth assessment report of the intergovernmental panel on climate change \(chap. 9\). Cambridge University Press, https://doi.org/10.1017/9781009157896.011, 2021.](https://doi.org/10.1017/9781009157896.011)

432 433 434 435 436

437 Găinușă-Bogdan, A., Swingedouw, D., Yiou, P., Cattiaux, J., Codron, F., and Michel, S.: AMOC and summer sea ice  
438 as key drivers of the spread in mid-holocene winter temperature patterns over Europe in PMIP3 models, Global  
439 Planet. Change., 184, <https://doi.org/10.1016/j.gloplacha.2019.103055>, 2020.

440 Ganopolski, A., Kubatzki, C., Claussen, M., Brovkin, V., and Petoukhov, V.: The Influence of Vegetation-  
441 Atmosphere-Ocean Interaction on Climate During the Mid-Holocene, *Science*, 280, 1916-1919,  
442 <https://doi.org/10.1126/science.280.5371.1916>, 1998.

443 Held, I. M.: The Partitioning of the Poleward Energy Transport between the Tropical Ocean and Atmosphere, *J.*  
444 *Atmos. Sci.*, 58, 943-948, [https://doi.org/10.1175/1520-0469\(2001\)058<0943:Tpotpe>2.0.Co;2](https://doi.org/10.1175/1520-0469(2001)058<0943:Tpotpe>2.0.Co;2), 2001.

445 Hunke, E. C. and Lipscomb, W. H.: CICE: The Los Alamos Sea Ice Model documentation and software user's  
446 manual, version 4.1. Doc. LACC-06-012, 76, [CICE documentation and software user's manual.pdf](https://colorado.edu)  
447 ([colorado.edu](https://colorado.edu)), 2010.

448 Jiang, D., Lang, X., Tian, Z., and Wang, T.: Considerable Model–Data Mismatch in Temperature over China during  
449 the Mid-Holocene: Results of PMIP Simulations, *J. Climate*, 25, 4135-4153, <https://doi.org/10.1175/jcli-d-11-00231.1>, 2012.

450 Jiang, Z., Brierley, C., Thornalley, D., and Sax, S.: No changes in overall AMOC strength in interglacial PMIP4 time  
451 slices, *Clim. Past*, 19, 107-121, <https://doi.org/10.5194/cp-19-107-2023>, 2023a.  
452 [Jiang, Z., Brierley, C. M., Bader, J., Braconnot, P., Erb, M., Hopcroft, P. O., Jiang, D., Jungclaus, J., Khon, V.,](https://doi.org/10.5194/cp-19-107-2023)  
453 [Lohmann, G., Marti, O., Osman, M. B., Otto-Bliesner, B., Schneider, B., Shi, X., Thornalley, D. J. R., Tian, Z.,](https://doi.org/10.5194/cp-19-107-2023)  
454 [and Zhang, Q.: No Consistent Simulated Trends in the Atlantic Meridional Overturning Circulation for the Past](https://doi.org/10.5194/cp-19-107-2023)  
455 [6,000 Years, Geophysical Research Letters](https://doi.org/10.5194/cp-19-107-2023), 50, e2023GL103078, <https://doi.org/10.1029/2023GL103078>, 2023b.

456 Jin, G.: Mid-Holocene climate change in North China, and the effect on cultural development, *Chinese Sci. Bull.*, 47,  
457 <https://doi.org/10.1360/02tb9095>, 2002.

458 Joussaume, S. and Taylor, K.: Status of the paleoclimate modeling intercomparison project (PMIP), *World*  
459 *Meteorological Organization-Publications-WMO TD*, 425-430, 1995.

460 Kageyama, M., Braconnot, P., Harrison, S. P., Haywood, A. M., Jungclaus, J. H., Otto-Bliesner, B. L., Peterschmitt,  
461 J.-Y., Abe-Ouchi, A., Albani, S., Bartlein, P. J., Brierley, C., Crucifix, M., Dolan, A., Fernandez-Donado, L.,  
462 Fischer, H., Hopcroft, P. O., Ivanovic, R. F., Lambert, F., Lunt, D. J., Mahowald, N. M., Peltier, W. R., Phipps, S.,  
463 J., Roche, D. M., Schmidt, G. A., Tarasov, L., Valdes, P. J., Zhang, Q., and Zhou, T.: The PMIP4 contribution to  
464 CMIP6 – Part 1: Overview and over-arching analysis plan, *Geosci. Model. Dev.*, 11, 1033-1057,  
465 <https://doi.org/10.5194/gmd-11-1033-2018>, 2018.

466 [Larrasoña, J.: A Northeast Saharan Perspective on Environmental Variability in North Africa and its Implications for](https://doi.org/10.5194/gmd-11-1033-2018)  
467 [Modern Human Origins, Modern Origins: A North African Perspective](https://doi.org/10.5194/gmd-11-1033-2018), 19-34, 10.1007/978-94-007-2929-2\_2,

468 [2012.](https://doi.org/10.5194/gmd-11-1033-2018)

470 Lawrence, D. M., Oleson, K. W., Flanner, M. G., Fletcher, C. G., Lawrence, P. J., Levis, S., Swenson, S. C., and  
471 Bonan, G. B.: The CCSM4 Land Simulation, 1850–2005: Assessment of Surface Climate and New Capabilities,  
472 *J. Climate*, 25, 2240-2260, <https://doi.org/10.1175/jcli-d-11-00103.1>, 2012.

473 Liu, Z., Zhu, J., Rosenthal, Y., Zhang, X., Otto-Bliesner, B. L., Timmermann, A., Smith, R. S., Lohmann, G., Zheng,  
474 W., and Elison Timm, O.: The Holocene temperature conundrum, *P. Natl. Acad. Sci. USA*, 111, E3501-3505,  
475 <https://doi.org/10.1073/pnas.1407229111>, 2014.

476 Monnin, E., Indermühle, A., Daellenbach, A., Flückiger, J., Stauffer, B., Stocker, T. F., Raynaud, D., and Barnola,  
477 J.-M.: Atmospheric CO<sub>2</sub> Concentrations over the Last Glacial Termination, *Science*, 291, 112-114,  
478 <https://doi.org/10.1126/science.291.5501.112>, 2001.

479 Monnin, E., Steig, E. J., Siegenthaler, U., Kawamura, K., Schwander, J., Stauffer, B., Stocker, T. F., Morse, D. L.,  
480 Barnola, J.-M., Bellier, B., Raynaud, D., and Fischer, H.: Evidence for substantial accumulation rate variability in  
481 Antarctica during the Holocene, through synchronization of CO<sub>2</sub> in the Taylor Dome, Dome C and DML ice  
482 cores, *Earth Planet. Sc. Lett.*, 224, 45-54, <https://doi.org/10.1016/j.epsl.2004.05.007>, 2004.

483 Moss, M. L., Peteet, D. M., and Whitlock, C.: Mid-Holocene culture and climate on the Northwest Coast of North  
484 America, in: *Climate Change and Cultural Dynamics*, 491-529, <https://doi.org/10.1016/b978-012088390-5.50019-4>, 2007.

486 Otto-Bliesner, B. L., Brady, E. C., Clauzet, G., Tomas, R., Levis, S., and Kothavala, Z.: Last Glacial Maximum and  
487 Holocene Climate in CCSM3, *J. Climate*, 19, 2526-2544, <https://doi.org/10.1175/jcli3748.1>, 2006.

488 Otto-Bliesner, B. L., Braconnot, P., Harrison, S. P., Lunt, D. J., Abe-Ouchi, A., Albani, S., Bartlein, P. J., Capron, E.,  
489 Carlson, A. E., Dutton, A., Fischer, H., Goelzer, H., Govin, A., Haywood, A., Joos, F., LeGrande, A. N.,  
490 Lipscomb, W. H., Lohmann, G., Mahowald, N., Nehrbass-Ahles, C., Pausata, F. S. R., Peterschmitt, J.-Y.,  
491 Phipps, S. J., Renssen, H., and Zhang, Q.: The PMIP4 contribution to CMIP6 – Part 2: Two interglacials,  
492 scientific objective and experimental design for Holocene and Last Interglacial simulations, *Geosci. Model. Dev.*,  
493 10, 3979-4003, <https://doi.org/10.5194/gmd-10-3979-2017>, 2017.

494 Park, S., Bretherton, C. S., and Rasch, P. J.: Integrating Cloud Processes in the Community Atmosphere Model,  
495 Version 5, *J. Climate*, 27, 6821-6856, <https://doi.org/10.1175/jcli-d-14-00087.1>, 2014.

496 Rahmstorf, S.: Thermohaline Ocean Circulation, in: *Encyclopedia of Quaternary Sciences*, edited by: Elias, S. A.,  
497 Elsevier, Amsterdam, 1–10, 2006.

498 Roberts, N., Eastwood, W. J., Kuzucuoğlu, C., Fiorentino, G., and Caracuta, V.: Climatic, vegetation and cultural  
499 change in the eastern Mediterranean during the mid-Holocene environmental transition, *The Holocene*, 21, 147-  
500 162, <https://doi.org/10.1177/0959683610386819>, 2011.

501 Rossignol-Strick, M.: The Holocene climatic optimum and pollen records of sapropel 1 in the eastern Mediterranean,  
502 9000–6000BP, *Quaternary Sci. Rev.*, 18, 515-530, [https://doi.org/10.1016/S0277-3791\(98\)00093-6](https://doi.org/10.1016/S0277-3791(98)00093-6), 1999.

503 Sandweiss, D. H., Maasch, K. A., and Anderson, D. G.: Transitions in the Mid-Holocene, *Science*, 283, 499-500,  
504 <https://doi.org/10.1126/science.283.5401.499>, 1999.

505 Shi, X. and Lohmann, G.: Simulated response of the mid-Holocene Atlantic meridional overturning circulation in  
506 ECHAM6-FESOM/MPIOM, *J. Geophys. Res.-Oceans*, 121, 6444-6469, <https://doi.org/10.1002/2015jc011584>,  
507 2016.

508 Shi, X., Werner, M., Wang, Q., Yang, H., and Lohmann, G.: Simulated Mid-Holocene and Last Interglacial Climate  
509 Using Two Generations of AWI-ESM, *J. Climate*, 35, 4211-4231, <https://doi.org/10.1175/jcli-d-22-0354.1>,  
510 2022. [Smith, R. S. and Gregory, J. M.: A study of the sensitivity of ocean overturning circulation and climate to  
511 freshwater input in different regions of the North Atlantic, \*Geophys. Res. Lett.\*, 36,  
512 <https://doi.org/10.1029/2009gl038607>, 20](https://doi.org/10.1029/2009gl038607)

513 [Smith, R. and Gent, P.: The Parallel Ocean Program \(POP\) reference manual, Los Alamos Unclassified Report LA-  
514 UR-02-2484, 2010.](https://doi.org/10.1029/2009gl038607)

515 Trenberth, K. E. and Caron, J. M.: Estimates of Meridional Atmosphere and Ocean Heat Transports, *J. Climate*, 14,  
516 3433-3443, [https://doi.org/10.1175/1520-0442\(2001\)014<3433:Eomaa>2.0.Co;2](https://doi.org/10.1175/1520-0442(2001)014<3433:Eomaa>2.0.Co;2), 2001.

517 Wanner, H., Beer, J., Bütkofer, J., Crowley, T. J., Cubasch, U., Flückiger, J., Goosse, H., Grosjean, M., Joos, F.,  
518 Kaplan, J. O., Küttel, M., Müller, S. A., Prentice, I. C., Solomina, O., Stocker, T. F., Tarasov, P., Wagner, M.,  
519 and Widmann, M.: Mid- to Late Holocene climate change: an overview, *Quaternary Sci. Rev.*, 27, 1791-1828,  
520 <https://doi.org/10.1016/j.quascirev.2008.06.013>, 2008.

521 Warden, L., Moros, M., Neumann, T., Shennan, S., Timpson, A., Manning, K., Sollai, M., Wacker, L., Perner, K.,  
522 Häusler, K., Leipe, T., Zillén, L., Kotilainen, A., Jansen, E., Schneider, R. R., Oeberst, R., Arz, H., and Sinnighe  
523 Damsté, J. S.: Climate induced human demographic and cultural change in northern Europe during the mid-  
524 Holocene, *Sci. Rep-UK*, 7, <https://doi.org/10.1038/s41598-017-14353-5>, 2017.

525 Williams, C. J. R., Guarino, M.-V., Capron, E., Malmierca-Vallet, I., Singarayer, J. S., Sime, L. C., Lunt, D. J., and  
526 Valdes, P. J.: CMIP6/PMIP4 simulations of the mid-Holocene and Last Interglacial using HadGEM3:

527 comparison to the pre-industrial era, previous model versions and proxy data, *Clim. Past*, 16, 1429-1450,  
528 <https://doi.org/10.5194/cp-16-1429-2020>, 2020.

529 Wunsch, C.: The Total Meridional Heat Flux and Its Oceanic and Atmospheric Partition, *J. Climate*, 18, 4374-4380,  
530 <https://doi.org/10.1175/jcli3539.1>, 2005.

531 Yan, M. and Liu, J.: Physical processes of cooling and mega-drought during the 4.2 ka BP event: results from  
532 *TraCE-21ka* simulations, *Clim. Past*, 15, 265-277, <https://doi.org/10.5194/cp-15-265-2019>, 2019.

533 Zhang, J., Kong, X., Zhao, K., Wang, Y., Liu, S., Wang, Z., Liu, J., Cheng, H., and Edwards, R. L.: Centennial-scale  
534 climatic changes in Central China during the Holocene climatic optimum, *Palaeogeogr. Palaeoclimatol.*  
535 *Palaeoecol.*, 558, <https://doi.org/10.1016/j.palaeo.2020.109950>, 2020.

536 Zhang, M., Liu, Y., Zhang, J., and Wen, Q.: AMOC and Climate Responses to Dust Reduction and Greening of  
537 Sahara during the Mid-Holocene, *J. Climate*, 1-59, <https://doi.org/10.1175/jcli-d-20-0628.1>, 2021a.

538 Zhang, Q., Berntell, E., Axelsson, J., Chen, J., Han, Z., de Nooijer, W., Lu, Z., Li, Q., Zhang, Q., Wyser, K., and  
539 Yang, S.: Simulating the mid-Holocene, last interglacial and mid-Pliocene climate with EC-Earth3-LR, *Geosci.*  
540 *Model. Dev.*, 14, 1147-1169, <https://doi.org/10.5194/gmd-14-1147-2021>, 2021b.

541